Journal of Nuclear Materials 430 (2012) 239–245

Contents lists available at SciVerse ScienceDirect

Journal of Nuclear Materials

journal homepage: www.elsevier.com/locate/jnucmat

Reactions between water and vitreous silica during irradiation

Glenn K. Lockwood, Stephen H. Garofalini *

Interfacial Molecular Science Laboratory, Department of Materials Science and Engineering, Rutgers University, Piscataway, NJ 08854, United States

ARTICLE INFO

Article history:
Received 23 April 2012
Accepted 3 July 2012
Available online 16 July 2012

ABSTRACT

Molecular dynamics simulations were conducted to determine the response of a vitreous silica surface in contact with water to radiation damage. The defects caused by radiation damage create channels that promote high H^+ mobility and result in significantly higher concentration and deeper penetration of H^+ in the silica subsurface. These subsurface H^+ hop between acidic sites such as $SiOH_2^+$ and Si–(OH)–Si until subsequent radiation ruptures siloxane bridges and forms subsurface non-bridging oxygens (NBOs); existing excess H^+ readily bonds to these NBO sites to form SiOH. The high temperature caused by irradiation also promotes the diffusion of molecular H_2O into the subsurface, and although H_2O does not penetrate as far as H^+, it readily reacts with ruptured bridges to form 2SiOH. These SiOH sites are thermally stable and inhibit the reformation of bridges that would otherwise occur in the absence of water. In addition to this reduction of self-healing, the presence of water during the self-irradiation of silica may cause an increase in the glass's proton conductivity.

1. Introduction

Vitrification is recognized as a key component to the immobilization and long-term storage of radioactive wastes, and borosilicate-based glasses have become an international standard in developing waste glass compositions. These borosilicate glasses are particularly attractive because of their ability to be loaded to a high degree with a wide range of waste products, their relative resistance to radiation damage, and the technological maturity of glass processing [1,2]. However, given the very long lifetimes of some of the radionuclides involved (typically given to be a range from 100,000 to 1,000,000 years for high-level waste [3]), some percentage of waste forms must be expected to fail during this service life.

As a result of this, the predominant mechanism for radionuclide release to the biosphere will be through dissolution of the waste form into groundwater in waste repositories [4], and significant work has been done in studying how radiation damage affects dissolution and leaching rates in such waste glass materials. Unfortunately, the results from these experiments have often yielded contradictory results ranging from irradiation increasing dissolution rates [5–7] to having negligible effects [8–11], underscoring the need to explore how radiation damage affects the interactions between water and glass at a more fundamental level.

Molecular dynamics (MD) simulations are well suited to studying the effects of radiation in vitreous silica [12] and have been used for this purpose for over a decade [13]. As computational power has increased, the models used have also progressed to utilize much more realistic kinetic energies of recoil nuclei [14], to devise novel techniques to enable simulation of much larger systems [15], and to increase compositional accuracy [15]. These advancements have revealed a wealth of information on how silicate waste forms degrade under irradiation at the atomistic level; however, these simulations have never included water or considered its effect.

Given the important role of water in the dissolution and degradation of glassy waste forms, including water in these molecular models of damage mechanisms is of critical importance to establishing a comprehensive, fundamental understanding of how glassy waste forms will degrade. To this end, the authors recently conducted MD simulations that included hydroxyls and water in bulk vitreous silica and found that the presence of water accelerates the accumulation of residual structural damage in the form of non-bridging oxygen and larger voids in the glassy network [16]. Based on this observed propensity for water to limit self-healing of radiation-damaged silica and increase the concentration of voids under irradiation, it is easy to envision radiation damage causing voids and channels at the surface, providing a new pathway for the accelerated diffusion of water into silica. This would then lead to further damage accumulation, ingress of water, and an overall accelerated degradation of the silica network.

The interactions between water and small voids and channels are also relevant beyond the scope of waste glasses. For example, abnormally high proton conduction has been observed in mesoporous silica [17–20], and evidence suggests that defects play a significant role in H^+ mobility in water–silica systems [21–25]. Given the fact that ballistic radiation creates large concentrations of defects in silica, it is not unreasonable to consider how radiation damage affects the mobility of H^+ at the silica surface and into the bulk

* Corresponding author.
E-mail address: shg@rutgers.edu (S.H. Garofalini).

0022-3115/$ - see front matter © 2012 Elsevier B.V. All rights reserved.
http://dx.doi.org/10.1016/j.jnucmat.2012.07.004

glass. Despite this, very little work has been done towards understanding how radiation damage affects proton conductivity in water–silica systems.

The study presented here explores the processes of H^+ and H_2O transport into silica under irradiation more directly by modeling a vitreous silica surface in contact with liquid water and simulating the effects of recoil nuclei in the silica subsurface. By simulating the self-irradiation of silica near a water–silica interface and using an interatomic potential that allows water to dissociate, the effects of both the water–silica reactions during the radiation damage process and the damaged region on accelerated water penetration and degradation of the silica have been observed within a single simulated system.

2. Computational methods

2.1. Interatomic potential

A dissociative interatomic potential for water was used in this study to model the interactions between all atoms. This model benefits from being able to reproduce the behavior of bulk water, bulk silica, and the water–silica interface in terms of structure, chemistry, transport processes, energetics, and other properties [21,23,26,27]. It also has been used previously to simulate the effects of irradiation in silica [16] and to reproduce the characteristic rapid formation of damage followed by picosecond-scale healing produced by other MD models [13,28]. Despite this wide range of applicability, it is a relatively simple potential comprised of two- and three-body interactions and takes the form:

$$U_{ij}^{2-body}(r_{ij}) = U_{ij}^{q-q} + U_{ij}^{qd-qd} + U_{ij}^{q-qd} + U_{ij}^{qd-q} + U_{ij}^{rep} + U_{ij}^{disp} + U_{ij}^{12} \quad (1)$$

where each energy term is a function of the interatomic spacing r_{ij} and is given by:

$$U_{ij}^{q-q}(r_{ij}) = \frac{q_i q_j}{r_{ij}} \cdot \mathrm{erfc}\left(\frac{r_{ij}}{\beta}\right) \quad (2)$$

$$U_{ij}^{qd-qd}(r_{ij}) = \frac{q_i^d q_j^d}{r_{ij}} \mathrm{erf}\left(\frac{r_{ij}}{2\xi_{ij}}\right) \cdot \mathrm{erfc}\left(\frac{r_{ij}}{\beta}\right) \quad (3)$$

$$U_{ij}^{q-q^d}(r_{ij}) = \frac{q_i q_j^d}{r_{ij}} \mathrm{erf}\left(\frac{r_{ij}}{\sqrt{2}\xi_{ij}}\right) \cdot \mathrm{erfc}\left(\frac{r_{ij}}{\beta}\right) \quad (4)$$

$$U_{ij}^{q^d-q}(r_{ij}) = \frac{q_i^d q_j}{r_{ij}} \mathrm{erf}\left(\frac{r_{ij}}{\sqrt{2}\xi_{ij}}\right) \cdot \mathrm{erfc}\left(\frac{r_{ij}}{\beta}\right) \quad (5)$$

$$U_{ij}^{rep}(r_{ij}) = A_{ij}^{rep} \frac{2\xi_{ij}^r}{r_{ij}} \mathrm{erfc}\left(\frac{r_{ij}}{2\xi_{ij}^r}\right) \quad (6)$$

$$U_{ij}^{disp}(r_{ij}) = -\frac{C_{ij}^6}{r_{ij}^6} \quad (7)$$

$$U_{ij}^{12}(r_{ij}) = +\frac{B_{ij}^{12}}{r_{ij}^{12}} \quad (8)$$

The parameters used in this study are listed in Table 1. The calculated interactions between pairs are limited to atoms separated by a distance less than $R_c = 1.0$ nm, and as in past work, the long-range Coulomb interactions are determined by use of the Wolf summation method [29] with a decay parameter of $\beta = 0.446$ nm. The point charges q_i are partial charges and defined such that $q_{Si} = +1.808$, $q_O = -0.5q_{Si}$, and $q_H = +0.25q_{Si}$. The diffuse charges are defined by the simple, empirical relationship $q_i^d = -0.25q_i$. Eq. (8) is used to eliminate spurious attractive forces that might occur at very short range during collisions rather than the ZBL [30] term often used. ZBL assumes full ionic charges and simple point charges in its empirical fit, whereas we use partial charges and include diffuse charges in our potential so its incorporation would be problematic.

Table 1
Two-body potential parameters. The ξ_{O-H}^r parameter is calculated as a function of temperature and pressure as described elsewhere [26].

i–j Pair	A_{ij}^{rep} (fJ)	ξ_{ij} (nm)	ξ_{ij}^r (nm)	B_{ij}^{12} (J nm^{12})	C_{ij}^6 (J nm^6)
O–H	0.2283	2.4	$f(T, P)$	0	0
O–O	0.0425	2.4	0.06100	4.0780×10^{-31}	4.2260×10^{-24}
H–H	0.0000	2.4	0.00000	0	0
Si–O	0.2670	2.4	0.03730	3.5000×10^{-31}	7.0000×10^{-24}
Si–Si	0.0700	2.4	0.06400	0	0
Si–H	0.5000	2.4	0.03500	5.6486×10^{-32}	3.8000×10^{-24}

The three-body component of the interatomic potential is a Stillinger–Weber type function that serves to provide an energetic bias of certain j–i–k triplets towards certain angles, empirically equivalent to the effects introduced by partial bond covalency (as in SiO_2) or lone pairs (as in H_2O). It takes the form:

$$U_{jik}^{3-body}(r_{ij}, r_{ik}, \theta_{jik}) = \lambda_{jik} exp\left(\frac{\gamma_{ij}}{r_{ij} - r_{ij}^0} + \frac{\gamma_{ik}}{r_{ik} - r_{ik}^0}\right)(cos\theta_{jik} - cos\theta_{jik}^0)^2 \quad (9)$$

and the parameters used here are listed in Table 2.

2.2. System assembly

The starting configuration for the systems simulated in this study was comprised of a slab of amorphous silica ($10.44 \times 10.44 \times 5$ nm) in contact with a film of liquid water (about 2 nm) with about 5.5 nm of vacuum above, resulting in a system size of $10.44 \times 10.44 \times 12.51$ nm. The silica slab contained 36,678 atoms and the water film contained 21,900 atoms.

To generate the silica slab, a simulation box of 10.50 nm on each side was filled with 25,537 Si atoms and 51,074 O atoms placed at random, then simulated at 6000 K for 15 ps in the canonical ensemble (constant number of atoms, volume, and temperature) followed by 15 ps in the microcanonical ensemble (constant number of atoms, volume, and energy). From this temperature, the system was quenched to a temperature of 300 K via intermediate steps in a manner identical to previous work [21].

Once equilibrated to 300 K, the system was then simulated under constant temperature and pressure (or constant N–P–T, where $N = 76{,}611$ atoms, $T = 298$ K, $P = 1$ atm) for 40 ps. The zero-strain dimensions of the silica sample were assumed to be equal to the average dimensions taken over the final 20 ps of this 40 ps simulation; thus, after the 40 ps of N–P–T simulation, the final atomic configuration was rescaled in the x, y, and z dimensions to these average dimensions of 10.44 nm in x, y, and z. All atoms above $z = 5.009$ nm were then removed to maintain the large x–y surface

Table 2
Three-body potential parameters.

j–i–k Triplet	λ_{jik} (fJ)	γ_{ij} (nm)	γ_{ik} (nm)	r_{ij}^0 (nm)	r_{ik}^0 (nm)	θ_{jik}^0
O–Si–O	0.0150	0.28	0.28	0.30	0.30	109.5
Si–O–Si	0.0010	0.20	0.20	0.28	0.28	109.5
H–O–H	0.0300	0.13	0.13	0.16	0.16	100.0
Si–O–H	0.0050	0.20	0.12	0.28	0.15	109.5

area but reduce the unnecessarily large size of the SiO_2 sample. The resulting system was an amorphous, stoichiometric SiO_2 slab containing 36,678 atoms with dimensions x_L = 10.44 nm and y_L = 10.44 nm, and with a height of 5.009 nm in z.

The water film was generated by randomly inserting 7300 H_2O molecules between z = 5.3 nm and z = 8.3 nm such that no randomly inserted H_2O molecule was within 0.2 nm of any previously inserted H_2O molecule. Following this, the velocities of all atoms in the resulting system were randomized to a Gaussian distribution corresponding to T = 298.0 K. The bottom 0.5 nm of the system was frozen, and this system was simulated at 298.0 K for 20 ps under the canonical ensemble to allow the randomly placed water to condense to liquid density and hydroxylate the SiO_2 surface.

The final configuration of this 20 ps simulation, hereafter referred to as the "starting configuration," was then subjected to the irradiation procedure detailed below.

2.3. Irradiation

The overall method of simulating self-irradiation in the glass was similar to the methods used in the past [12–14,16,28,31,32]. To simulate the ballistic effects of an alpha decay, an oxygen atom was first chosen at random from a volume bounded by 2.0 nm $< x < (x_L - 2.0\text{ nm})$, 2.0 nm $< y < (y_L$ 2.0 nm), and $(z_S - 3.5\text{ nm}) < z < (z_S - 2.5\text{ nm})$, where x_L and y_L are the simulation box length in x and y, and z_S is the z position of the water/silica interface. This primary knock-on atom (PKA) was given an additional +1 keV of kinetic energy in the +z direction, and the system was allowed to evolve for 2 ps before another oxygen was randomly chosen and the process repeated. The depth of this irradiated zone was chosen based on observations in past work that oxygen ions with 1 keV of kinetic energy travel, on average, between 2.5 nm and 3.5 nm [16]. While the amorphous network introduces significant variability to the length of individual defect tracks, this choice provided the maximum probability of collision cascades ending at the silica surface rather than in the subsurface or passing into the liquid water.

Due to the very high atomic velocities immediately following the initiation of these PKAs, the integration time step was allowed to vary such that the maximum displacement of any atom between consecutive system configurations, Δr_{max}, always remained between 0.12 pm $< \Delta r_{max} <$ 1.2 pm; the time step was scaled up by a factor of five or down by a factor of 10 to satisfy this criterion, and these maximum displacements were checked after every tenth iteration. Although the time step was allowed to vary between successive iterations of the entire system, the same time step was always used to calculate the trajectories of all atoms within each step.

To counteract the large amount of momentum introduced with each simulated PKA, the atoms occupying the bottom 0.5 nm of the system were frozen and not allowed to move. This was found to be sufficient to prevent the system from forming any net momentum. Similarly, the large amounts of kinetic energy put into the system were allowed to dissipate through the atoms residing 0.3 nm above this frozen layer by rescaling their velocities every tenth iteration to coincide with T = 298.0 K. Finally, all three directions in the system were periodic; although the simulation was nominally aperiodic in the z direction, reflective boundaries would have had the potential to reflect high-energy particles back down at the surface and obfuscate the effects of self-irradiation. By preserving periodic boundaries in z, any high-energy atoms that reached z_L would simply be braked by the frozen 0.5 nm of glass and cause no additional damage to the glass after it had left the surface.

The "hit-and-relax" process of initiating a PKA and then allowing the system to relax for 2 ps was repeated seventeen times for a total of 34.0 ps of irradiation. An initial 2 ps of simulation preceded this hit-and-relax process, resulting in a total simulation time of 36.0 ps.

3. Results

In the results that follow, NBOs are defined as oxygen atoms bonded to exactly one silicon atom at a distance $r_{Si-O} < 0.2$ nm; NBOs may or may not be protonated and exist as SiOH, $SiOH_2^+$, or SiO^-. Hydrogen is considered bonded to an oxygen if $r_{O-H} < 0.12$ nm. Oxygen atoms bonded to exactly two silicon atoms will be hereafter referred to as bridges, and bridges supporting an adsorbed proton, Si–(OH)–Si, will be referred to as "bridging OH" or simply "BOH" to be consistent with past studies [21]. In describing the irradiation process, each initiation of a PKA will be referred to as a "hit;" the simulation presented here consisted of seventeen hits.

3.1. Radiation-induced alteration of the SiO_2 network

Each hit resulted in the rupture of bridges, causing the rapid formation of NBOs and complementary undercoordinated Si sites. In the majority of cases, these complementary defects recombined, resulting in significant structural recovery during the 2 ps following each hit (Fig. 1). This healing is incomplete though, and there is a net decrease in bridging oxygen concentration over the course of the 36 ps of irradiation; this behavior is consistent with previous findings [16,28].

This accumulation of damage was found to occur in a region of the defect track after much of the initial recoil energy had already dissipated, and these observations are consistent with past irradiation studies of vitreous silica [14]. This region of reduced bridge density is apparent when comparing the spatial distribution of bridges before and after irradiation (Fig. 2a) and resides between 0.7 nm and 0.3 nm below the water–silica interface. The choice to irradiate the volume described in Section 2.3 was made with the intent of the collision cascades ending just beneath the interface though, and as such, the location of this region of maximum damage was anticipated.

Fig. 1 shows a slight decrease in curvature for t > 28 ps which is evidence of defect saturation [28]. However, examining the x–y distribution of the PKA oxygen locations and the defects they form (Fig. 3) reveals that neither the PKA position nor the defects they cause are uniformly distributed over the simulated surface. This is an artifact of the pseudorandom number generator employed for this simulation, and this localization of defects in the x–y plane causes the change in defect distribution in z (Fig. 2a) to be somewhat understated since each point in Fig. 2a represents the density over the entire x–y plane.

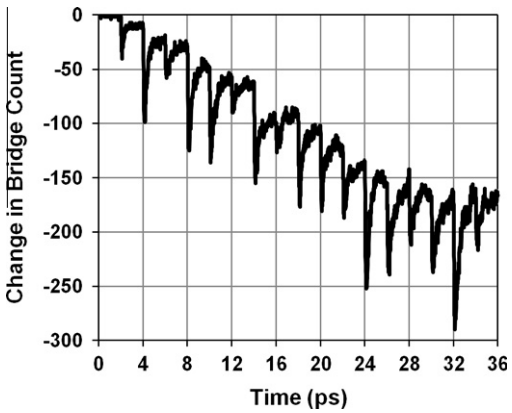

Fig. 1. Bridge formation over time.

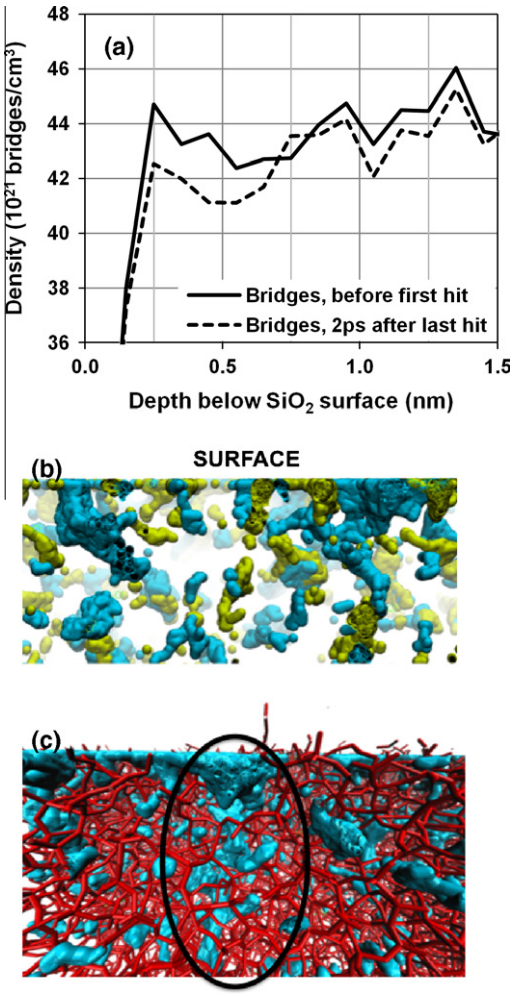

Fig. 2. (a) Density of bridging oxygen as a function of distance below the silica surface. (b) Side view of region showing interconnected void space less than 2.6 Å from any Si or O ions for pre-irradiated (yellow) and post-irradiated (blue) system, indicating more channel-like openings in latter. (c) Post-irradiated channel with red Si–O bonds included. Surface is at the top of (b) and (c) (water not shown). (For interpretation of the references to colour in this figure legend, the reader is referred to the web version of this article.)

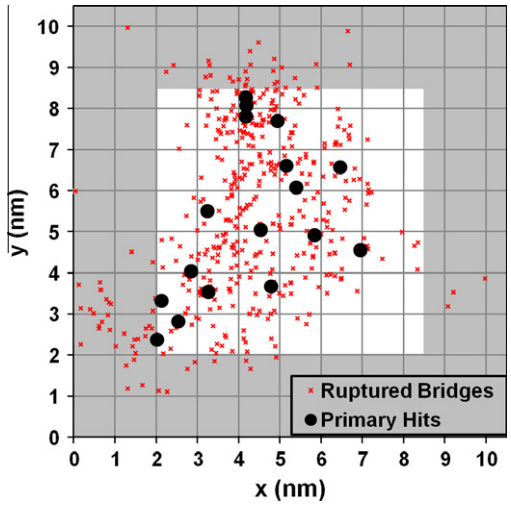

Fig. 3. Distribution of PKAs and consequent net damage in the *x*–*y* plane. All PKAs were chosen randomly from the non-shaded region. Ruptured bridges shown reflect the positions of bridges that ruptured following a decay event and did not re-form into a bridging site during the 2 ps following that decay.

In addition to changes in bridge concentration, radiation damage in silica can manifest in the form of changes in the ring size distribution [2]. Changes in this ring size distribution can occur independently of the bridge concentration since ruptured bridges readily recombine with any adjacent complementary defect and not necessarily their original neighbors. During the course of this irradiation simulation, a total of 397 rings with four, five, six, or seven silica members (which comprise the majority of rings in unirradiated bulk silica) were permanently destroyed. This destruction was offset by the net formation of 93 rings having eight or more members (i.e. small voids) and 15 three-membered rings (strained rings commonly found on silica surfaces). These changes in the ring size distribution are very similar to the observations of others who have utilized different interatomic potentials to model radiation damage in silica [33].

The observed net destruction of bridging oxygens (Fig. 1) and the loss of bridging oxygen density near the interface (Fig. 2a) are indicative of a net increase in free volume, a loss of density, and the formation of new surface in the irradiated region [2]. Also observed is the presence of interconnected void space, or 'channels', as shown in Fig. 2b and c that show side views of regions at and below the surface. To examine the spatial distribution of this interconnected void space in the pre-irradiated silica in comparison to the post-irradiated silica, a random space-filling procedure was carried out on the system configuration at the beginning of the irradiation simulation and after the 36 ps of irradiation. Positions less than 2.6 Å from any Si or O atom were generated randomly, filling space that enabled a view of interconnected channels into which water could penetrate. Fig. 2b shows that there are far fewer deep channels in the pre-irradiated (yellow) silica in comparison to the post-irradiated (blue) glass. Fig. 2c includes the Si–O bonds in another region containing a deep channel (~2 nm).

3.2. Water–silica reactions during irradiation

Water was found to readily react with the glassy network during the irradiation process as well, evidenced by a dramatic increase in SiOH concentration during irradiation. At the atomic configuration immediately preceding the first hit (t = 2.0 ps in Fig. 1), the system contained 476 SiOH sites which corresponds to a surface density of 4.37 SiOH/nm^2 and is consistent with experiment [34,35]. After seventeen hit-and-relax cycles (t = 36.0 ps), this concentration had increased to 977 SiOH.

These excess SiOH sites formed as bridges ruptured during the irradiation, producing a 3-coordinated $\equiv Si^+$ and $Si–O^-$ site and then reacting with H_2O (Fig. 4). The concentration of nonbridging oxygen (NBO) defects over time (solid line in Fig. 5) is complementary to the bridge concentration over time (Fig. 1); increases in NBO concentration mirror decreases in bridge concentration. However, decomposing this NBO concentration into protonated (Si–OH and $Si—OH_2^+$; shaded line in Fig. 5) and dry ($Si–O^-$; dotted line) sites reveals that the spikes in NBO concentration are caused by the formation of dry NBOs. These dry NBOs either heal back to bridging sites or form protonated NBOs very rapidly, and the net

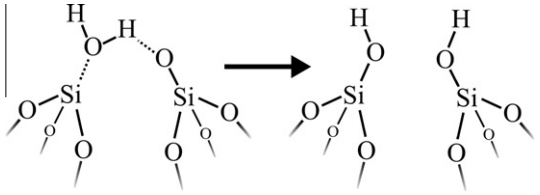

Fig. 4. Adsorption–dissociation reaction mechanism between H_2O and a ruptured bridge.

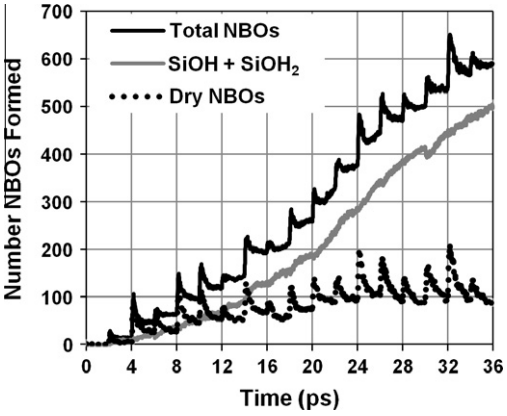

Fig. 5. Change in non-bridging defect concentration during irradiation.

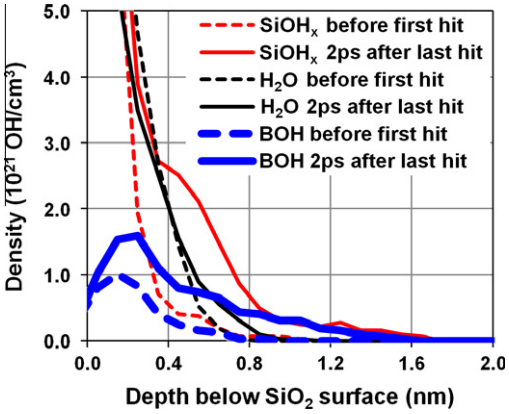

Fig. 7. Density and coordination of H as a function of distance into the silica subsurface before and after radiation damage.

change in dry NBO sites remains fairly constant over the time scale of the simulation.

Unlike the dry NBO concentration, the protonated NBO concentration increases steadily and shows no sharp changes coincident with each hit. This behavior is consistent with the long-held knowledge that clean, fresh silica surfaces are highly reactive with water [36], and once exposed, must be heated to ~900 °C to deprotonate the surface [34]. In the present results, water readily reacts with freshly exposed defects created in the collision cascades, but additional hits (and the accompanying increase in temperature) do not readily deprotonate these sites once formed. The net result is the steadily increasing concentration of $SiOH_x$ (where $x = 1$ or 2) sites.

3.3. Effect of radiation damage on subsurface H^+ concentrations

The distribution of H^+ in the silica subsurface is significantly altered as a result of irradiation, and this change is pronounced in the density profile of H^+ in the silica (Fig. 6). The concentration of subsurface H^+ increases at all depths below 0.3 nm, and integrating these two density profiles in Fig. 6 for depths greater than 0.3 nm indicates that this is an 86% increase in subsurface H^+. Additionally, the maximum depth of penetration increases during irradiation; the H^+ density profile goes to zero at a depth of 1.1 nm before irradiation and increases to 1.7 nm of penetration after.

Free H^+ is highly unstable and rapidly associates with neighboring O to form some type of OH in both H_2O and SiO_2 [24], and decomposing the hydrogen density function (Fig. 6) into contributions from various forms of OH (Fig. 7) reveals that the majority of the radiation-induced change in H^+ density depicted in Fig. 6 takes

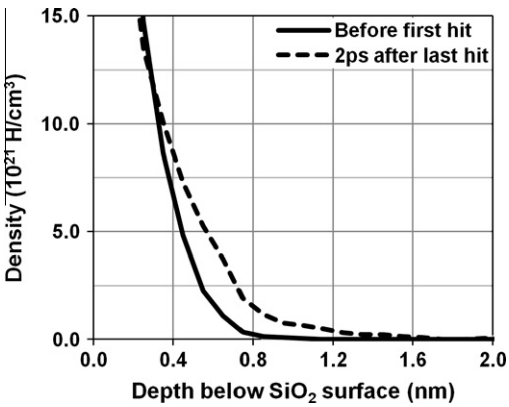

Fig. 6. Density of hydrogen in the silica subsurface.

the form of dissociatively chemisorbed water on the silica, not molecular H_2O. The concentration of $SiOH_x$ after irradiation (dashed red line in Fig. 7) deviates significantly from the sigmoidal shape of the pre-irradiated $SiOH_x$ density function (solid red line in Fig. 7); the irradiation caused a pocket of anomalously extensive $SiOH_x$ formation near the surface accompanied by an increase in $SiOH_x$ concentration of up to 10×. The position of this pocket coincides with the region of decreased bridging oxygen density at the surface (Fig. 2) and indicates that radiation damage plays a significant role in the formation of this highly depolymerized and hydroxylated near-surface region.

The deepest subsurface OH groups were a combination of $SiOH_x$ and bridging OH (or BOH) sites, and none of the original water was present as molecular H_2O at subsurface depths greater than 1.1 nm despite H^+ being present as deep as 1.7 nm. Additionally, no oxygens originally coordinated as H_2O were present at depths greater than 1.1 nm below the surface during irradiation. Thus, the deepest $SiOH_x$ sites observed did not form via the adsorption–dissociation reaction of the original H_2O as shown in Fig. 4; rather, they are the result of excess protons diffusing through the silica network from the near-surface reaction region (minor formation of H_2O from O in the silica occurs and will be discussed below). The excess H^+ on $SiOH_2^+$ and BOH sites are acidic and highly mobile [22–25,37], and this mobility facilitates the increase in both subsurface H^+ concentration and penetration depth.

The high mobility of these excess H^+ also provides a means to prevent healing of the network during the collision cascading despite the lack of H_2O to fuel the adsorption–dissociation reaction shown in Fig. 4. As bridges rupture and form NBOs, excess H^+ are free to hop to these NBOs to form SiOH, which are far less mobile and far more thermally stable, and inhibit the reformation of the ruptured bridge. While it is possible for SiOH to form a protonated bridge with a neighboring undercoordinated Si (i.e. $\equiv Si-OH + {}^+Si \equiv \rightarrow Si-[OH]-Si$), instances of this healing mechanism were found to be extremely rare relative to H^+ adsorption to deprotonated NBOs.

Oxygen ions originally incorporated in the silica network were found to transform into molecular H_2O in small quantities at depths as great as 1.0 nm below the surface as well. These H_2O molecules formed when network oxygen (either bridges or NBOs) were dislodged following a PKA and then quickly bonded to nearby excess H^+, highlighting a source of subsurface H_2O independent of H_2O diffusion from the surface. Once formed, they exhibit a range of expected behavior including molecular diffusion farther into the subsurface, participation in H^+ transport via H_3O^+ formation, and dissociative chemisorption on defect sites formed by subsequent PKAs.

3.4. Effect of elevated temperature

The average system temperature between hits was around 515 K towards the end of the irradiation simulation despite the 0.3 nm of atoms thermostated to 298.0 K. This temperature is within the range of conditions expected in waste repositories [38], and it is likely to have an effect on the kinetics of H_2O diffusion into the silica surface and how the subsurface H^+ concentration changes during irradiation. To this end, the irradiation simulation was repeated in the absence of irradiation; that is, the starting configuration for the irradiation simulation (see Section 2.2) was simulated for 36 ps within the canonical ensemble at 573 K, which is the upper limit of expected relevant repository temperatures [38]. The periodic boundary in z was replaced by a reflective boundary to prevent water vapor from interacting with the frozen underside of the silica component of the system.

This high-temperature, unirradiated simulation showed a greater subsurface concentration and a greater penetration depth of molecular H_2O when compared to the irradiated system. This suggests that the additional ingress of molecular H_2O observed during irradiation is largely a thermal effect and will occur regardless of whether or not the defect tracks caused by the collision cascades form channels to the silica surface. Thus, high repository temperatures make waste glasses susceptible to H_2O-induced inhibition of healing by providing a means for the passivation reaction depicted in Fig. 4 to occur in the subsurface. The fact that this unirradiated simulation was carried out at a constant, high temperature rather than the gradual increase in temperature experienced in the irradiated system precludes the absolute values of H_2O concentration from being directly compared, but these observations still hold qualitative importance.

Unlike the H_2O concentration, the $SiOH_x$ concentration increased only marginally in the absence of irradiation at 573 K. The $SiOH_x$ density profile retained its sigmoidal shape after the 36 ps of non-irradiation simulation, and it lacks the pocket of increased $SiOH_x$ concentration evident in the irradiated system (red line in Fig. 7). The penetration depth remains approximately constant as well. Thus, the increase in subsurface $SiOH_x$ observed after irradiation is not a thermal effect and arises as a result of radiation damage to the silica network near the water–silica interface.

4. Discussion

The presence of liquid water during the self-irradiation of silica has a definite adverse effect on the ability of silica to recover from radiation damage, and the irradiation process is accompanied by the ingress of a significant amount of H^+. The majority of these protons are bound in the form of SiOH, $SiOH_2^+$, or bridging OH, and they exist far deeper into the subsurface after irradiation than in systems not exposed to self-irradiation. However, H_2O molecules were unable to diffuse deep into the subsurface under the conditions simulated here, indicating that these deep protonated sites form as the result of the hopping of protons along radiation-induced defect channels. Additionally, a small concentration of deep subsurface H_2O forms as network oxygens are displaced from the network and capture excess protons.

These excess protons form near the water–silica interface as a result of either radiolysis or dissociative chemisorption (Fig. 4) on bridges ruptured as the collision cascade reaches the interface. Although these excess protons cannot passivate both halves of a ruptured bridge as depicted in Fig. 4, the high acidity of $SiOH_2^+$ and bridging OH sites allows these excess protons to rapidly move to non-bridging defects ($Si–O^-$) as they are formed by radiation damage. Once adsorbed to such a non-bridging site to form SiOH, that SiOH is very stable, and the incidences of SiOH reforming a bridge (whether it be a dry bridge or a protonated bridge) are very rare; the net result is permanent, residual depolymerization of the silica network and an opening of the network structure.

The 1 keV hits simulated here create defect regions with a large number of defect sites that are amenable to proton adsorption. Consequentially, protons rapidly diffuse along these defect tracks into the subsurface by hopping between adjacent defects [21,24,25], and these excess subsurface protons will readily passivate neighboring NBOs formed by subsequent collision cascades. The net result is the inhibition of structural healing in the subsurface caused by H^+; despite the fact that H_2O molecules were not able to diffuse down these defect tracks, their presence at the surface still caused increased damage accumulation away from the interface.

H^+ diffusion into the subsurface is analogous to proton conduction and suggests that radiation damage may increase the proton conductivity of silica near water–silica interfaces; similar phenomenon has been observed in mesoporous silica [17–20]. This effect would provide a means to directly measure the extent of the radiolytic damage of glass surfaces by measuring changes in conductivity. Additionally, radiation-induced enhanced proton conductivity may enable, in a fashion not unlike so-called radioparagenesis [39], the synthesis of proton-conductive glasses via radiation-induced structural modifications.

The high temperatures associated with radioactive waste glass promote the ingress of H_2O into the glass subsurface, and the radiation damage promotes the formation of SiOH. Since radioactive waste glasses are much more compositionally complicated than pure silica, the results shown here are perhaps indicative of a 'least reactive' case. In real waste glasses, the network modifier ions (alkali, alkaline earth, and other low cation field strength species) that are present would be more mobile than Si and allow for a more open network with modifier-rich channels as described in the 'modified continuous random network model' by Greaves [40], enabling enhanced leaching and reactions with moisture [2]. Because the mobility and passivating reactions of H_2O is dissimilar to $SiOH_2^+$/BOH, modeling the true degradation of repository waste glasses (whether it be via experiment or simulation) must account for both the high temperatures and the radiation damage simultaneously to capture the most realistic behavior. Experiments that irradiate silica glass under dry conditions before exposure to water will show (1) greater healing during irradiation and therefore a lower subsurface $SiOH_x$ and BOH concentration, and (2) lower concentrations of subsurface H_2O after exposure unless elevated temperature is maintained during water exposure. Behavior of complex waste glasses under such conditions would be more complicated because of the presence of modifier ions and multi-coordination species (such as B) in a manner that could only be conjectured at this point.

5. Conclusions

The presence of liquid water has a definite adverse effect on the ability of silica to recover from radiation damage, and the irradiation process results in significant ingress of H^+ into the silica subsurface. The high temperatures accompanying the irradiation of silica glass promotes the diffusion of molecular H_2O into the subsurface where it can passivate ruptured bridges via an adsorption–dissociation reaction, and the damage to the silica network as the result of collision cascades provides a defect channel along which rapid H^+ transport occurs. Excess H^+ in the deeper subsurface occurs in the form of $SiOH_2^+$ and Si–(OH)–Si, and the acidity of these sites allows them to rapidly react with any radiation-induced NBOs to form SiOH. Once formed, SiOH is very stable against both thermal deprotonation and reacting with undercoordinated Si to re-form bridges, causing an overall limited ability for vitreous silica to recover from radiation damage. Radiation damage may also increase the proton conductivity of hydrated silica via the formation of these acidic sites, suggesting that it

may be possible to quantify the radiolytic degradation of silica via conductivity measurements, and it may be possible to increase the proton conductivity of hydrated silica by exposing it to ballistic radiation.

Acknowledgement

G.K.L. gratefully acknowledges support from the Corning Foundation.

References

[1] W.E. Lee, M.I. Ojovan, M.C. Stennett, N.C. Hyatt, Adv. Appl. Ceram. 105 (2006) 3–12.
[2] W.J. Weber, R.C. Ewing, C.A. Angell, G.W. Arnold, A.N. Cormack, J.M. Delaye, D.L. Griscom, L.W. Hobbs, A. Navrotsky, D.L. Price, A.M. Stoneham, M.C. Weinberg, J. Mater. Res. 12 (1997) 1948–1978.
[3] I.S. Roxburgh, Geology of High Level Nuclear Waste Disposal, 1 ed., Chapman and Hall, London, 1987.
[4] I.W. Donald, B.L. Metcalfe, R.N.J. Taylor, J. Mater. Sci. 32 (1997) 5851–5887.
[5] J.C. Dran, M. Maurette, J.C. Petit, Science 209 (1980) 1518–1520.
[6] L.R. Pederson, G.L. McVay, J. Am. Ceram. Soc. 66 (1983) 863–867.
[7] W.J. Weber, Nucl. Instrum. Methods Phys. Res., Section B 32 (1988) 471–479.
[8] J. Wald, F. Roberts, Commun. Am. Ceram. Soc. (1984) C-69–C-70.
[9] D.M. Wellman, J.P. Icenhower, W.J. Weber, J. Nucl. Mater. 340 (2005) 149–162.
[10] S. Peuget, V. Broudic, C. Jégou, P. Frugier, D. Roudil, X. Deschanels, H. Rabiller, P.Y. Noel, J. Nucl. Mater. 362 (2007) 474–479.
[11] S. Peuget, J.-N. Cachia, C. Jegou, X. Deschanels, D. Roudil, V. Broudic, J.M. Delaye, J.-M. Bart, J. Nucl. Mater. 354 (2006) 1–13.
[12] J.M. Delaye, D. Ghaleb, Phys. Rev. B 61 (2000) 14481–14494.
[13] J.-M. Delaye, V. Louis-Achille, D. Ghaleb, J. Non-Cryst. Sol. 210 (1997) 232–242.
[14] J.-M. Delaye, D. Ghaleb, J. Nucl. Mater. 348 (2006) 243–255.
[15] J.M. Delaye, D. Ghaleb, Phys. Rev. B 71 (2005) 224204.
[16] G.K. Lockwood, S.H. Garofalini, J. Nucl. Mater. 400 (2010) 73–78.
[17] M. Nogami, R. Nagao, C. Wong, J. Phys. Chem. 102 (1998) 5772–5775.
[18] M. Nogami, Y. Abe, Phys. Rev. B 55 (1997) 12108–12112.
[19] M. Nogami, J. Sol–Gel Sci. Technol. 31 (2004) 359–364.
[20] Y. Aoki, H. Habazaki, S. Nagata, A. Nakao, T. Kunitake, S. Yamaguchi, J. Am. Chem. Soc. 133 (2011) 3471–3479.
[21] G.K. Lockwood, S.H. Garofalini, J. Chem. Phys. 131 (2009) 074703.
[22] Y. Ma, A.S. Foster, R.M. Nieminen, Reactions and clustering of water with silica surface, J. Chem. Phys 122 (2005) 144709.
[23] T.S. Mahadevan, S.H. Garofalini, J. Phys. Chem. C 112 (2008) 1507–1515.
[24] H.A. Kurtz, S.P. Karna, IEEE Trans. Nucl. Sci. 46 (1999) 1574–1577.
[25] K. Vanheusden, P.P. Korambath, H.A. Kurtz, S.P. Karna, D.M. Fleetwood, W.M. Shedd, R.D. Pugh, IEEE Trans. Nucl. Sci. 46 (1999) 1562–1567.
[26] T.S. Mahadevan, S.H. Garofalini, J. Phys. Chem. B 111 (2007) 8919–8927.
[27] S.H. Garofalini, T.S. Mahadevan, S. Xu, G.W. Scherer, ChemPhysChem 9 (2008) 1997–2001.
[28] A. Kubota, M.-J. Caturla, J. Stolken, B. Sadigh, S. Reyes, T. Diaz de la Rubia, J.F. Latkowski, Nucl. Instrum. Methods Phys. Res. B 202 (2003) 88–92.
[29] D. Wolf, P. Keblinski, S.R. Phillpot, J. Eggebrecht, J. Chem. Phys. 110 (1999) 8254–8282.
[30] J.F. Ziegler, J.P. Biersack, U. Littmark, The Stopping and Range of Ions in Matter, Pergamon, New York, 1985.
[31] J.-M. Delaye, D. Ghaleb, Nucl. Instrum. Methods Phys. Res., Section B 153 (1999) 157–162.
[32] A. Kubota, M.-J. Caturla, S.A. Payne, T. Diaz de la Rubia, J.F. Latkowski, J. Nucl. Mater. 307–311 (2002) 891–894.
[33] F. Mota, M.-J. Caturla, J.M. Perlado, J. Molla, A. Ibarra, J. Nucl. Mater. 386–388 (2009) 75–78.
[34] R.K. Iler, The Chemistry of Silica, John Wiley and Sons, New York, 1979.
[35] L.T. Zhuravlev, Langmuir 3 (1987) 316–318.
[36] C.J. Brinker, R.K. Brow, D.R. Tallant, R.J. Kirkpatrick, J. Non-Cryst. Solids 120 (1990) 26–33.
[37] L.J. Criscenti, J.D. Kubicki, S.L. Brantley, J. Phys. Chem. A 110 (2006) 198–206.
[38] Site characterization plan, Yucca mountain site, nevada research and development area, Nevada DOE/RW-0199, in: Office of Civilian Waste Management, U.S. Department of Energy, Washington, D.C., 1988, pp. 8.3.5.9–51.
[39] C. Jiang, C. Stanek, N. Marks, K. Sickafus, B. Uberuaga, Philos. Mag. Lett. 90 (2010) 435–446.
[40] G.N. Greaves, A. Fontaine, P. Lagarde, D. Raoux, S.J. Gurman, Nature 293 (1981) 611–616.